URN (Paper): urn:nbn:de:gbv:ilm1-2011iwk-052:3

56TH INTERNATIONAL SCIENTIFIC COLLOQUIUM
Ilmenau University of Technology, 12 16 September 2011
URN: urn:nbn:gbv:ilm1-2011iwk:5

DEVELOPMENT AND COMPARISON OF HIGH ORDER TOROIDAL FINITE ELEMENTS FOR CALCULATING DISC SPRINGS

Christoph Wehmann, Frank Rieg

University of Bayreuth
Department of Engineering Design and CAD
Universitätsstr. 30, 95440 Bayreuth

ABSTRACT

The present manuscript deals with the development and the application of toroidal finite elements. These finite elements belong to the class of curvilinear elements and, therefore, a special element formulation is required. This means to express stress, strain, and displacement in curvilinear coordinates. Here, an 8-node quadrilateral element is developed which is described by an isoparametric interpolation. The development of the governing equations is one main topic of this contribution. Another main topic is to evaluate the quality and efficiency of these elements with respect to the calculation of disc springs. In this context, calculations with toroidal elements are checked against experimental data which consists of load-deflection-curves. In addition, the effects of friction and differences to the exact rectangular cross section are considered. With the help of Riks procedure, characteristic curves with negative spring rates are obtained.

Index Terms— Toroidal finite elements, curvilinear coordinates, covariant derivatives, disc springs, geometrical nonlinearities

1. INTRODUCTION

Toroidal finite elements are very interesting in many applications of mechanical engineering.

They take advantage of a special symmetry, the rotational symmetry. Machine elements like disc springs or complete aggregates like pressure vessels feature this symmetry and, therefore, they are predestinated to be calculated by toroidal finite elements.
The present contribution deals with high order toroidal finite elements which are used for calculating disc springs. Disc springs are widely used in construction of machines, vehicles, and apparatus and their special mechanical behaviour requires numerical methods in order to calculate displacements and stresses.

2. BASIC MECHANICAL EQUATIONS

The basis for deriving a finite element formulation is represented by the equilibrium equations. Expressed by a variational principle, these equations can have the form of equation (1), compare [2]. This form results as the undeformed shape is used for referencing and the Lagrangian strain $\boldsymbol{\lambda}$ is choosen for describing the material behaviour. Like it is shown here, it is valid for static analysis without body forces.

$$\iiint_V \mathbf{S} \cdot \delta\boldsymbol{\lambda}\, dV = \iint_A \mathbf{t} \cdot \delta\mathbf{u}\, dA \qquad (1)$$

Herein $\mathbf{S}$ name the second Piola-Kirchhoff's stresses, $\delta\boldsymbol{\lambda}$ are the virtual Lagrangian strains, and $\delta\mathbf{u}$ are the virtual displacements. The stress vector is symbolized by $\mathbf{t}$. Choosing the undeformed shape as the reference-configuration means the Lagrangian way of referencing is applied. It follows that integration in left part of equation (1) has to be adopted to the volume V of the undeformed finite element respectively disc spring. In the same way, the surface integration in right part of equation (1) operates on the surface of the undeformed disc spring. This surface area A is the surrounding surface of the whole finite element model (here the model of the disc spring), excluding parts of this area with kinematic boundary conditions.

The Lagrangian strain $\boldsymbol{\lambda}$ can be obtained by considering a material line element and its change of quadrat of length. This change of length is shown in equation (2).

$$l^2 - L^2 = d\mathbf{x} \cdot d\mathbf{x} - d\mathbf{X} \cdot d\mathbf{X} \qquad (2)$$

By introducing the Lagrangian strain $\boldsymbol{\lambda}$ as a result of a Taylor's row (see (3)),

$$2\,\boldsymbol{\lambda} = \left(\frac{\partial \mathbf{x}}{\partial \mathbf{X}}\right)^T \frac{\partial \mathbf{x}}{\partial \mathbf{X}} - \mathbf{1} \qquad (3)$$

the change of length can be expressed as follows:

$$d\mathbf{x} \cdot d\mathbf{x} - d\mathbf{X} \cdot d\mathbf{X} = 2\, d\mathbf{X} \cdot \boldsymbol{\lambda} d\mathbf{X} \qquad (4)$$

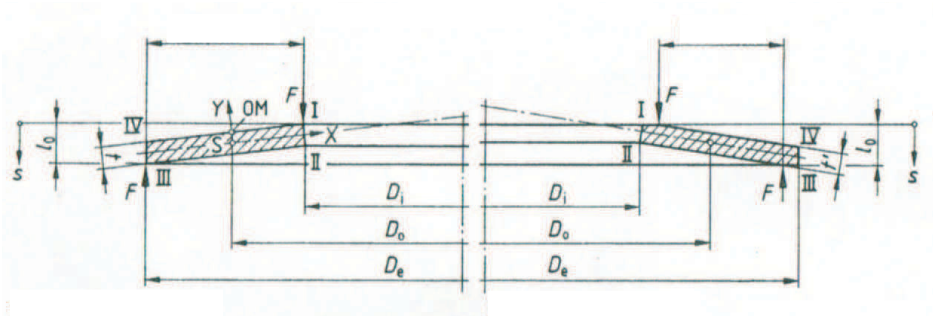

Fig. 1. Definitions of DIN 2092 [1] for describing disc springs

Recalling that $\mathbf{x} = \mathbf{X} + \mathbf{u}$, the Lagrangian strain can be expressed as it is displayed in (5). Here, it can be calculated from the displacement $\mathbf{u}$. The position of each material point at the undeformed configuration is symbolized by $\mathbf{X}$ and it yields that the displacement field $\mathbf{u}$ has to be formulated as a function of $\mathbf{X}$, $\mathbf{u} = \mathbf{u}(\mathbf{X})$.

$$\boldsymbol{\lambda} = \frac{1}{2}\left(\frac{\partial \mathbf{u}}{\partial \mathbf{X}} + \left(\frac{\partial \mathbf{u}}{\partial \mathbf{X}}\right)^T + \left(\frac{\partial \mathbf{u}}{\partial \mathbf{X}}\right)^T \frac{\partial \mathbf{u}}{\partial \mathbf{X}}\right) \tag{5}$$

Assuming that strains remain small, although displacements might be large, a linear relationship between stresses and strains can be applied. The corresponding constitutive equation is Hooke's law, which is shown in (6). Here, Hooke's law is generalized to the theory of large displacements.

$$\mathbf{S} = \mathbf{C}\,\boldsymbol{\lambda} \tag{6}$$

The introduced quantity $\mathbf{C}$ can be calculated by two material parameters, which are the Young's modulus E and the Poisson ratio ν.

3. FORMULATION IN CURVILINEAR COORDINATES

The special symmetry of toroidal elements requires to adapt the basic mechanical equations presented in section 2 to cylindrical coordinates. Therefore, the displacement field $\mathbf{u}$ needs to be expressed in these curvilinear coordinates as it is displayed in equation (7).

$$\mathbf{u} = u_r\,\mathbf{e}_r + u_\varphi\,\mathbf{e}_\varphi + u_z\,\mathbf{e}_z \tag{7}$$

In this equation u_r, u_φ, and u_z represent the displacements in $r-, \varphi-$, and $z-$direction, while $\mathbf{e}_r, \mathbf{e}_\varphi$, and $\mathbf{e}_z$ build up the corresponding coordinate basis.

Next, expressions for describing strain by cylindrical coordinates are derived. For that purpose, the following identity, taken from [3], is used.

$$\boldsymbol{\lambda} = \sum_{i,j} \lambda_{ij}\mathbf{e}_{ij} = \sum_{i,j} \Lambda_{ij}\mathbf{G}^{ij} \tag{8}$$

In equation (8) λ_{ij} denote the Lagrangian strains, measured in cartesian coordinates, whereas Λ_{ij} stands for the Lagrangian strains, measured in covariant coordinates. In this manner $\mathbf{e}_{ij}$ name the unit matrices of the cartesian basis and $\mathbf{G}^{ij}$ describe the unit matrices of the contravariant basis. Equation (9) and (10) give examples for both, the cartesian and the contravariant basis. Note that in (8) $\boldsymbol{\lambda}$ represents the matrix formulation of strain.

$$\mathbf{e}_{12} = \begin{bmatrix} 0 & 1 & 0 \\ 0 & 0 & 0 \\ 0 & 0 & 0 \end{bmatrix} \tag{9}$$

$$\mathbf{G}^{23} = \begin{bmatrix} G_1^2 G_1^3 & G_1^2 G_2^3 & G_1^2 G_3^3 \\ G_2^2 G_1^3 & G_2^2 G_2^3 & G_2^2 G_3^3 \\ G_3^2 G_1^3 & G_3^2 G_2^3 & G_3^2 G_3^3 \end{bmatrix} \tag{10}$$

By replacing the superscripts 2 and 3 in (10) through i and j, the general expression for $\mathbf{G}^{ij}$ is obtained. The items G_k^i of this resulting expression symbolize the coordinates of the unit vector $\mathbf{G}^i$, which belongs to the contravariant basis. The exact definition is shown in (11).

$$\mathbf{G}^i = \begin{bmatrix} G_1^i \\ G_2^i \\ G_3^i \end{bmatrix} = \begin{bmatrix} \frac{\partial \xi_i}{\partial X_1} \\ \frac{\partial \xi_i}{\partial X_2} \\ \frac{\partial \xi_i}{\partial X_3} \end{bmatrix} \tag{11}$$

The corresponding covariant basis vectors $\mathbf{G}_i$

$$\mathbf{G}_i = \begin{bmatrix} G_i^1 \\ G_i^2 \\ G_i^3 \end{bmatrix} = \begin{bmatrix} \frac{\partial X_1}{\partial \xi_i} \\ \frac{\partial X_2}{\partial \xi_i} \\ \frac{\partial X_3}{\partial \xi_i} \end{bmatrix} \tag{12}$$

behave inverse to $\mathbf{G}^i$, what means that their dot product become one or zero and can be expressed by the Kronecker-symbol. Thus, equation (13) follows, compare [4].

$$\mathbf{G}_i \cdot \mathbf{G}^j = \delta_{ij} \tag{13}$$

3.1. Strain measurement in covariant coordinates

With the help of a Taylor's row, an infinitesimal material line element $d\mathbf{X}$ can be expressed by the covariant basis, compare equation (14).

$$d\mathbf{X} = \sum_i \mathbf{G}_i d\xi_i \tag{14}$$

Next, it is shown that the coefficients Λ_{ij} are applicable to measure strain in covariant coordinates. Therefore, (14) and (8) are inserted into (4). Combining the result with (2) yields to equation (15).

$$2\,d\mathbf{X}\cdot\boldsymbol{\lambda}d\mathbf{X} = 2\sum_{i,j,k,l}\mathbf{G}_i d\xi_i\cdot\Lambda_{jk}\mathbf{G}^{jk}\mathbf{G}_l d\xi_l \tag{15}$$

Applying (11) and the general form of (10), the matrix vector product in equation (15) will simplify according to (16) if relation (13) is accounted.

$$\mathbf{G}^{jk}\mathbf{G}_l = \mathbf{G}^j\delta_{kl} \tag{16}$$

Finally, after using (13) a second time, equation (17) is obtained.

$$2\,d\mathbf{X}\cdot\boldsymbol{\lambda}d\mathbf{X} = 2\sum_{i,j} d\xi_i\Lambda_{ij}d\xi_j \tag{17}$$

This relation points out that the coefficients Λ_{ij} are suitable for describing strain in covariant coordinates. In order to get a calculation rule for these coefficients, it is required to express (2) by (14). The resulting equation is presented in (18).

$$l^2 - L^2 = \sum_{ij}\left(\frac{\partial\mathbf{x}}{\partial\xi_i}\cdot\frac{\partial\mathbf{x}}{\partial\xi_j} - \frac{\partial\mathbf{X}}{\partial\xi_i}\cdot\frac{\partial\mathbf{X}}{\partial\xi_j}\right)d\xi_i d\xi_j \tag{18}$$

Accounting that $\mathbf{x} = \mathbf{X} + \mathbf{u}$, equation (18) yields to (19).

$$\begin{aligned} l^2 - L^2 = \sum_{ij}\Bigg(&\frac{\partial\mathbf{X}}{\partial\xi_i}\cdot\frac{\partial\mathbf{u}}{\partial\xi_j} + \frac{\partial\mathbf{u}}{\partial\xi_i}\cdot\frac{\partial\mathbf{X}}{\partial\xi_j} \\ &+\frac{\partial\mathbf{u}}{\partial\xi_i}\cdot\frac{\partial\mathbf{u}}{\partial\xi_j}\Bigg)d\xi_i d\xi_j \end{aligned} \tag{19}$$

Next, the definition of the covariant basis (12) is inserted to achieve equation (20).

$$\begin{aligned} l^2 - L^2 = \sum_{ij}\Bigg(&\mathbf{G}_i\cdot\frac{\partial\mathbf{u}}{\partial\xi_j} + \frac{\partial\mathbf{u}}{\partial\xi_i}\cdot\mathbf{G}_j \\ &+\frac{\partial\mathbf{u}}{\partial\xi_i}\cdot\frac{\partial\mathbf{u}}{\partial\xi_j}\Bigg)d\xi_i d\xi_j \end{aligned} \tag{20}$$

The partial derivatives in (20) have to be expressed by components related to the covariant coordinate basis in order to calculate the dot products efficiently. Therefore, the general form of partial derivation in curvilinear coordinates (21) which is taken from [4] is applied.

$$\frac{\partial\mathbf{u}}{\partial\xi_i} = \sum_{kl}\left(\frac{\partial u^k}{\partial\xi_i} + \Gamma^k_{li}u^l\right)\mathbf{G}_k \tag{21}$$

Therein the coefficients Γ^k_{li} are commonly known as Christoffel-symbols. Concerning cylinder coordinates, they are listed in [4] and this source is used hereafter. Comparing (2), (4), and (17) the formula (22) for calculating strain in covariant coordinates is found. Below, the explicit expression of Λ_{11} will be developed step by step, while the other coordinates of $\boldsymbol{\lambda}$ will be limited to compact presentation.

$$\Lambda_{ij} = \frac{1}{2}\left(\mathbf{G}_i\cdot\frac{\partial\mathbf{u}}{\partial\xi_j} + \frac{\partial\mathbf{u}}{\partial\xi_i}\cdot\mathbf{G}_j + \frac{\partial\mathbf{u}}{\partial\xi_i}\cdot\frac{\partial\mathbf{u}}{\partial\xi_j}\right) \tag{22}$$

Because the covariant basis is orthogonal when using cylinder coordinates, the coordinate Λ_{11} reduces to (23), accounting equation (21).

$$\begin{aligned} \Lambda_{11} = \frac{1}{2}\sum_k\Bigg(&\left(\frac{\partial u^1}{\partial\xi_1} + \Gamma^1_{k1}u^k\right)G_{11} \\ &+\left(\frac{\partial u^1}{\partial\xi_1} + \Gamma^1_{k1}u^k\right)G_{11} \\ &+\sum_l\left(\frac{\partial u^l}{\partial\xi_1} + \Gamma^l_{k1}u^k\right)^2 G_{ll}\Bigg) \end{aligned} \tag{23}$$

The quantities G_{ll} symbolize dot products as it is illustrated below.

$$G_{ll} = \mathbf{G}_l\cdot\mathbf{G}_l \tag{24}$$

Their values in case of cylinder coordinates (25) are taken from [4].

$$G_{11} = 1,\ G_{22} = r^2,\ G_{33} = 1 \tag{25}$$

Furthermore the following Christoffel-symbols are required.

$$\begin{aligned} \Gamma^1_{11} = \Gamma^1_{21} = \Gamma^1_{31} = 0 \\ \Gamma^2_{11} = 0,\ \Gamma^2_{21} = \frac{1}{r},\ \Gamma^2_{31} = 0 \\ \Gamma^3_{11} = \Gamma^3_{21} = \Gamma^3_{31} = 0 \end{aligned} \tag{26}$$

Finally, it is necessary to transform the contravariant coordinates of displacement and substitute the derivatives with respect to ξ_i by derivatives with respect to r, φ, and z.

$$\begin{aligned} u^1 = u_r,\ u^2 = \frac{u_\varphi}{r},\ u^3 = u_z \\ \frac{\partial}{\partial\xi_1} = \frac{\partial}{\partial r},\ \frac{\partial}{\partial\xi_2} = \frac{\partial}{\partial\varphi},\ \frac{\partial}{\partial\xi_3} = \frac{\partial}{\partial z} \end{aligned} \tag{27}$$

Altogether, this yields to equation (28), which is ready for discretization by finite elements.

$$\begin{aligned} \Lambda_{11} = \frac{\partial u_r}{\partial r} + \frac{1}{2}\Bigg(&\left(\frac{\partial u_r}{\partial r}\right)^2 + \left(\frac{\partial u_\varphi}{\partial r}\right)^2 \\ &+\left(\frac{\partial u_z}{\partial r}\right)^2\Bigg) \end{aligned} \tag{28}$$

The other coordinates Λ_{ij} can be developed similarly, the resulting expressions are shown below.

$$\Lambda_{22} = r\,\frac{\partial u_\varphi}{\partial \varphi} + r\,u_r + \frac{1}{2}\left(\left(\frac{\partial u_r}{\partial \varphi} - u_\varphi\right)^2 + \left(\frac{\partial u_\varphi}{\partial \varphi} + u_r\right)^2 + \left(\frac{\partial u_z}{\partial \varphi}\right)^2\right) \tag{29}$$

$$\Lambda_{33} = \frac{\partial u_z}{\partial z} + \frac{1}{2}\left(\left(\frac{\partial u_r}{\partial z}\right)^2 + \left(\frac{\partial u_\varphi}{\partial z}\right)^2 + \left(\frac{\partial u_z}{\partial z}\right)^2\right) \tag{30}$$

$$\Lambda_{12} = \Lambda_{21} = \frac{1}{2}\left(\frac{\partial u_r}{\partial \varphi} - u_\varphi + r\,\frac{\partial u_\varphi}{\partial r} + \frac{\partial u_r}{\partial r}\left(\frac{\partial u_r}{\partial \varphi} - u_\varphi\right) + \frac{\partial u_\varphi}{\partial r}\left(\frac{\partial u_\varphi}{\partial \varphi} + u_r\right) + \frac{\partial u_z}{\partial r}\,\frac{\partial u_z}{\partial \varphi}\right) \tag{31}$$

$$\Lambda_{23} = \Lambda_{32} = \frac{1}{2}\left(r\,\frac{\partial u_\varphi}{\partial z} + \frac{\partial u_z}{\partial \varphi} + \frac{\partial u_r}{\partial z}\left(\frac{\partial u_r}{\partial \varphi} - u_\varphi\right) + \frac{\partial u_\varphi}{\partial z}\left(\frac{\partial u_\varphi}{\partial \varphi} + u_r\right) + \frac{\partial u_z}{\partial \varphi}\,\frac{\partial u_z}{\partial z}\right) \tag{32}$$

$$\Lambda_{31} = \Lambda_{13} = \frac{1}{2}\left(\frac{\partial u_z}{\partial r} + \frac{\partial u_r}{\partial z} + \frac{\partial u_r}{\partial z}\,\frac{\partial u_r}{\partial r} + \frac{\partial u_\varphi}{\partial z}\,\frac{\partial u_\varphi}{\partial r} + \frac{\partial u_z}{\partial z}\,\frac{\partial u_z}{\partial r}\right) \tag{33}$$

3.2. Strain measurement in physical coordinates

Concerning cylinder coordinates, there are three different possibilities to define the coordinate basis. It can be defined by the contravariant basis, the covariant basis or the physical basis. The advantage of the contravariant basis and the covariant basis is their common mathematical handling. Considering the treatment of the derivatives in equation (21), it would be almost impossible to use the physical basis. However, the contravariant basis and the covariant basis also have a disadvantage, which forces to switch to the physical basis. The lengths of the basis vectors aren't one, the basis vectors aren't unit vectors [4]. By contrast, the basis vectors of the physical basis are unit vectors.

This is why coordinates of the strain $\boldsymbol{\lambda}$ finally have to be expressed related to the physical basis. Otherwise it would be impossible to gain a formulation of the basic equation (1), which is reduced to a pure coordinate formulation. Such a formulation is required for implementation in a finite element code.

The general transformation rules between covariant and physical coordinates are given in [4]. These rules are applied hereafter to the Lagrangian strain $\boldsymbol{\lambda}$.

$$\begin{aligned} &\Lambda^r_{rr} = \Lambda_{11},\ \Lambda^r_{\varphi\varphi} = \frac{1}{r^2}\,\Lambda_{22},\ \Lambda^r_{zz} = \Lambda_{33} \\ &\Lambda^r_{r\varphi} = \frac{1}{r}\,\Lambda_{12},\ \Lambda^r_{\varphi z} = \frac{1}{r}\,\Lambda_{23},\ \Lambda^r_{zr} = \Lambda_{31} \end{aligned} \tag{34}$$

The superscript r in equation (34) denotes that these quantities belong to the physical coordinate basis. With the help of these transformation rules, the strain coordinates related to the physical basis can be obtained as following.

$$\Lambda^r_{rr} = \frac{\partial u_r}{\partial r} + \frac{1}{2}\left(\left(\frac{\partial u_r}{\partial r}\right)^2 + \left(\frac{\partial u_\varphi}{\partial r}\right)^2 + \left(\frac{\partial u_z}{\partial r}\right)^2\right) \tag{35}$$

$$\Lambda^r_{\varphi\varphi} = \frac{1}{r}\,\frac{\partial u_\varphi}{\partial \varphi} + \frac{1}{r}\,u_r + \frac{1}{2}\,\frac{1}{r^2}\left(\left(\frac{\partial u_r}{\partial \varphi} - u_\varphi\right)^2 + \left(\frac{\partial u_\varphi}{\partial \varphi} + u_r\right)^2 + \left(\frac{\partial u_z}{\partial \varphi}\right)^2\right) \tag{36}$$

$$\Lambda^r_{zz} = \frac{\partial u_z}{\partial z} + \frac{1}{2}\left(\left(\frac{\partial u_r}{\partial z}\right)^2 + \left(\frac{\partial u_\varphi}{\partial z}\right)^2 + \left(\frac{\partial u_z}{\partial z}\right)^2\right) \tag{37}$$

$$\Lambda^r_{r\varphi} = \Lambda^r_{\varphi r} = \frac{1}{2}\,\frac{1}{r}\left(\frac{\partial u_r}{\partial \varphi} - u_\varphi + r\,\frac{\partial u_\varphi}{\partial r} + \frac{\partial u_r}{\partial r}\left(\frac{\partial u_r}{\partial \varphi} - u_\varphi\right) + \frac{\partial u_\varphi}{\partial r}\left(\frac{\partial u_\varphi}{\partial \varphi} + u_r\right) + \frac{\partial u_z}{\partial r}\,\frac{\partial u_z}{\partial \varphi}\right) \tag{38}$$

$$\Lambda^r_{\varphi z} = \Lambda^r_{z\varphi} = \frac{1}{2}\,\frac{1}{r}\left(r\,\frac{\partial u_\varphi}{\partial z} + \frac{\partial u_z}{\partial \varphi} + \frac{\partial u_r}{\partial z}\left(\frac{\partial u_r}{\partial \varphi} - u_\varphi\right) + \frac{\partial u_\varphi}{\partial z}\left(\frac{\partial u_\varphi}{\partial \varphi} + u_r\right) + \frac{\partial u_z}{\partial \varphi}\,\frac{\partial u_z}{\partial z}\right) \tag{39}$$

$$\Lambda^r_{zr} = \Lambda^r_{rz} = \frac{1}{2}\left(\frac{\partial u_z}{\partial r} + \frac{\partial u_r}{\partial z} + \frac{\partial u_r}{\partial z}\,\frac{\partial u_r}{\partial r} + \frac{\partial u_\varphi}{\partial z}\,\frac{\partial u_\varphi}{\partial r} + \frac{\partial u_z}{\partial z}\,\frac{\partial u_z}{\partial r}\right) \tag{40}$$

3.3. Material behaviour and calculation of stresses

Having obtained the equations for Lagrangian strain coordinates related to the physical basis of the cylinder coordinate system, the material behaviour has to be specified in order to get equations for calculating stresses. By choosing the physical coordinate basis for strains and stresses, the magnitudes of the several strain and stress components are completely stored in their coordinates and this is why it is sufficient to express the material equations directly in coordinates of strains and stresses. The corresponding basis matrices which are shown for example in (8), can be cutted out. Concerning the material behaviour, Hooke's law is applied to connect Lagrangian strain and second Piola-Kirchhoff's stress. Second Piola-Kirchhoff's stress has to be taken, because it is work-conjugated with the Lagrangian strain, compare [3]. In literature, this constitutive equation which results from a generalization of Hooke's law to the theory of large displacements is also named St. Venant's law [2]. In classical linear theory of elasticity, the cartesian coordinates of stress and strain are simply replaced by the corresponding physical cylinder coordinates to get the Hooke's law in cylinder coordinates. If the Lagrangian strain coordinates are related to the physical cylinder coordinate basis, it will be possible to do the same in nonlinear elasticity. Using Lamé's parameters, Hooke's law becomes (41).

$$S_{ij}^r = \lambda \left(\Lambda_{rr}^r + \Lambda_{\varphi\varphi}^r + \Lambda_{zz}^r \right) \delta_{ij} + 2\,\mu\,\Lambda_{ij}^r \qquad (41)$$

Therein λ and μ symbolize Lamé's parameters, which are defined by (42), see [6]. They can be used instead of Young's modulus E and Poisson's ratio ν.

$$\lambda = \frac{E\,\nu}{(1-2\,\nu)\,(1+\nu)} \qquad \mu = \frac{E}{2\,(1+\nu)} \qquad (42)$$

4. FINITE ELEMENT DISCRETIZATION

This chapter deals with the development of an 8-node toroidal element for numerical solving of the curvilinear mechanical formulation above. The following section is based on theory and implementation of the Z88-element torus no. 8 [5]. First of all, the same shape functions N_i are used to interpolate displacements. Because of the rotational symmetry, the integration in φ-direction can be done analytical and a two-dimensional discretization is sufficient for modeling disc springs or other machine elements with the same symmetry. Accordingly, the displacement (7) simplifies to (43) and every node has two degrees of freedom.

$$\mathbf{u} = u_r\,\mathbf{e}_r \;+\; u_z\,\mathbf{e}_z \qquad (43)$$

Figure 2 illustrates shape, node position, and coordinate system orientation of the applied Z88-element torus no. 8.

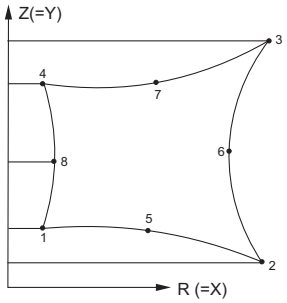

Fig. 2. Toroidal element No. 8 of Z88 [5]

It follows that the shape functions for interpolation of displacements look like equation (44) displays.

$$u_r = \sum_k N_k u_r^k\,, \quad u_z = \sum_k N_k u_z^k \qquad (44)$$

Next, stresses and strains are expressed in Z88-notation (45) for toroidal elements.

$$\mathbf{S} = \begin{bmatrix} S_{rr}^r \\ S_{zz}^r \\ S_{rz}^r \\ S_{\varphi\varphi}^r \end{bmatrix}, \quad \boldsymbol{\lambda} = \begin{bmatrix} \Lambda_{rr}^r \\ \Lambda_{zz}^r \\ \Lambda_{rz}^r \\ \Lambda_{\varphi\varphi}^r \end{bmatrix} \qquad (45)$$

Because of the symmetry (46), the coordinates $\Lambda_{r\varphi}$ and $\Lambda_{\varphi z}$ disappear. Due to the isotropic material behaviour the corresponding stress coordinates $S_{r\varphi}$ and $S_{\varphi z}$ become zero, too.

$$\frac{\partial}{\partial\varphi}(\cdot\cdot) = 0, \;\; u_\varphi = 0 \qquad (46)$$

Introducing the displacement-strain transformation matrix $\mathbf{B}$,

$$\mathbf{B} = \frac{\partial \boldsymbol{\lambda}}{\partial \mathbf{u}} \qquad (47)$$

where $\mathbf{u}$ stands for the nodal displacement vector, leads to following form of the equilibrium equations (1).

$$\iiint_V \mathbf{S}^T\,\mathbf{B}\,dV\,\delta\boldsymbol{u} = \mathbf{F}^T\,\delta\mathbf{u} \qquad (48)$$

In addition, the nodal force vector $\mathbf{F}$ is introduced in (48). Finally, by demanding (48) to be valid for arbitrary variations $\delta\mathbf{u}$, the algebraic equation (49) is obtained.

$$\iiint_V \mathbf{B}^T\,\mathbf{S}\,dV = \mathbf{F} \qquad (49)$$

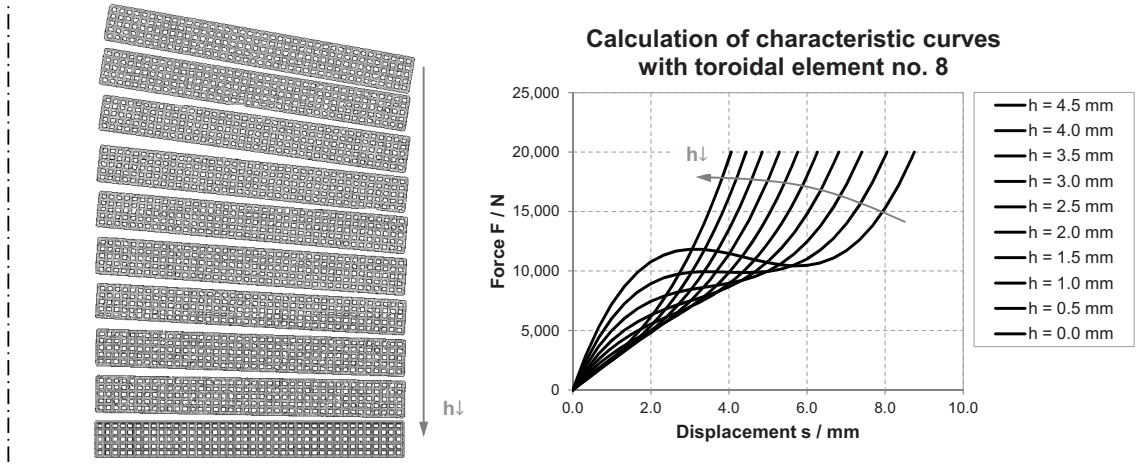

Fig. 3. Characteristic curves of disc springs with different heights, calculated by torus no. 8

The next chapter deals with the numerical solution of this equation by using Newton-Raphson's and Riks procedures.

5. CALCULATION OF DISC SPRINGS

In this chapter, the toroidal element developed above is applied to several disc springs. These disc springs differ from their height h, which is the distance in s-direction between points II and III (see figure 1). The other geometrical parameters are shown in (50).

$$\begin{aligned} D_e = 100.0mm,\ D_i = 51.0mm \\ t = 2.7mm \end{aligned} \tag{50}$$

For discretization of this structures the mapped mesher Z88N is used, who generates the meshes on the left of figure 3. Each of these meshes contains 200 toroidal elements, five in axial direction and 40 in radial direction. Disc springs with small heights $h \leq 2.5\,mm$ can be calculated by Newton-Raphson-procedure, while for springs with larger heights the procedure of Riks is required. This characteristic is reasoned by the negative spring rate of disc springs with large heights h. The Newton-Raphson-procedure is not capable of overcoming points near to the local maximum, because it is controled by applied force. The same problem is observed by Niepage, who suggests to use a procedure controled by displacement [7]. In this context, the procedure of Riks can be applied. It is controled by a given arc length increment, which can be a force increment, a displacement increment or a composition of force and displacement increment. It follows that Riks procedure enables calculating characteristic curves up to high forces and displacements for disc springs with negative spring rates, too. Concerning the material parameters on which the calculations of figure 3 are based, the following values for Young's modulus E and Poisson's ratio ν are used.

$$E = 210,000\,N/mm^2,\ \nu = 0.29 \tag{51}$$

On the left side of figure 3, the different finite element meshes are shown. Toroidal elements greatly simplify modeling of disc springs: only the cross section has to be meshed. With regard to the boundary conditions, one force and one given displacement exist. The force is applied to the node on point I, while the displacement of the node on point III (see figure 1) is set to zero.

6. EXPERIMENT

The quality of the results obtained by the presented toroidal element will be checked against experimental data in chapter 7. Here, it is illustrated, how this experimental data is gained. The disc spring is loaded by a hydraulic system, while bearing and loading only is applied to a small annular surface. Thus, high deflections, which are larger than h, can be reached. Measurement of force is performed by a load cell, which is placed between hydraulic cylinder and disc spring. A dial indicator is used to measure the deflection of point I.

7. COMPARISON OF CALCULATION AND EXPERIMENT

This chapter deals with the results of the measured and calculated characteristic curves of the disc spring (52).

$$\begin{aligned} D_e = 100.0mm,\ D_i = 51.0mm \\ t = 2.7mm,\ h = 3.5mm \\ E = 206,000N/mm^2,\ \nu = 0.3 \end{aligned} \tag{52}$$

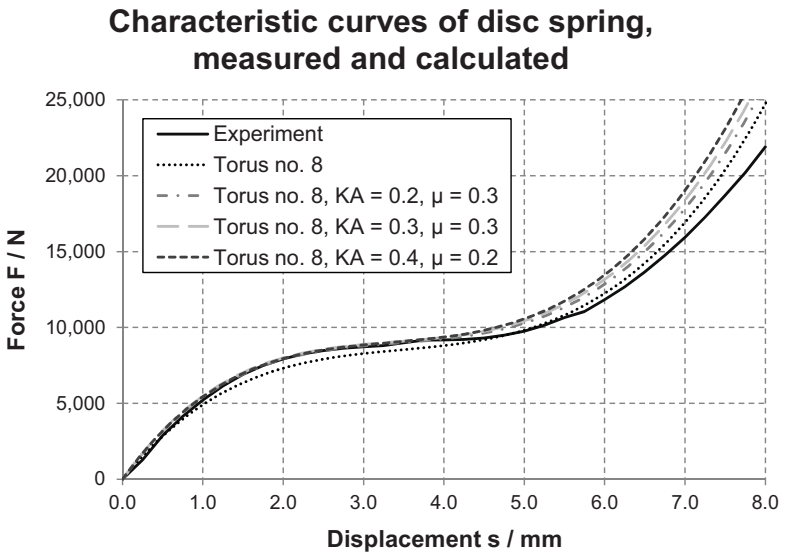

Fig. 4. Measured characteristic curve compared to calculations with torus no. 8, taken from [8] (modified)

Figure 4 illustrates the corresponding characteristic curves. The last three curves, labeled by "KA" and "μ" take additional boundary conditions into account. One of these conditions is a displacement of the applied force and the bearing reasoned by a difference to the exact rectangular cross section. Actually, the corners of disc springs have small roundings and, hence, the applied force acts further outwards, while the bearing is located further inwards. The displacement of force and bearing position is labeled KA and measured in mm, so KA = 0.2 means a displacement of 0.2 mm.

The other additional boundary condition is a friction force, which acts radially on the outer diameter. The corresponding friction parameter μ which is used for the calculations is shown in figure 4. The results point out that with these additional effects the characteristic curve can be calculated exactly up to a deflection of $s \approx h \approx 3.5mm$. Without accounting roundings and friction, the stiffness at $s < h$ is less than measured.

At higher deflections $s > h$, all curves lay upside the measured data, whether additional boundary conditions are accounted or not.

8. CONCLUSION AND OUTLOOK

In terms of development toroidal elements are sophisticated and require finite element formulation in curvilinear coordinates. The corresponding set up of equations is presented in this paper. Having implemented an 8-node quadrilateral element based on Z88 element type no. 8, calculation results with high qualities are obtained. Due to the application of finite element calculation, it is possible to account additional boundary conditions, which leads to nearly exact characteristic curves up to deflections $s \approx h$.

At higher deflections $s > h$ the calculated stiffness is higher than observed experimentally. This probably might be explained by inelastic material behaviour. With regard to applications of disc springs accounting inelastic processes might be of less interest, but with regard to maufacturing processes, it is an important topic for further research.

9. REFERENCES

[1] DIN 2092 *Tellerfedern. Berechnung*, Beuth, Berlin, 1992

[2] Wriggers, P. *Nichtlineare Finite-Element-Methoden*, Springer, Berlin, 2001

[3] Parisch, H. *Festkörperkontinuumsmechanik. Von den Grundgleichungen zur Lösung mit Finiten Elementen*, Teubner, Stuttgart, 2003

[4] Neemann, K.; Schade, H. *Tensoranalysis*, de Gruyter, Berlin, 2006

[5] Rieg, F.; Hackenschmidt, R. *Finite Elemente Analyse für Ingenieure, Eine leicht verständliche Einführung*, Hanser, München, Wien, 2009

[6] Landau, L. D.; Lifschitz, E. M. *Lehrbuch der theoretischen Physik, Band VII, Elastizitätstheorie*, Akademie Verlag, Berlin, 1991

[7] Niepage, P. *Vergleich verschiedener Verfahren zur Berechnung von Tellerfedern*, Draht 34, S. 105 - 108, 251 - 255, 1983

[8] Zimmermann, M. *Anwendung der Finite-Elemente-Analyse zur Ermittlung nichtlinearer Federkennlinien*, Diplomarbeit, Universität Bayreuth, 2011